Atmospheric
Chemistry
and Physics
Discussions

Open Access

Modelling and assimilation of lidar signals over Greater Paris during the MEGAPOLI summer campaign

Y. Wang[1,2], K. N. Sartelet[1], M. Bocquet[1,3], and P. Chazette[2]

[1]CEREA, joint laboratory École des Ponts ParisTech – EDF R& D, Université Paris-Est, 77455 Champs-sur-Marne, France
[2]LSCE, joint laboratory CEA-CNRS, UMR8212, 91191 Gif-sur-Yvette, France
[3]INRIA, Paris-Rocquencourt Research Center, Le Chesnay, France

Correspondence to: Y. Wang (wangy@cerea.enpc.fr) and M. Bocquet (bocquet@cerea.enpc.fr)

Discussion Paper | Discussion Paper | Discussion Paper | Discussion Paper

ACPD

13, 27115–27161, 2013

Comparison of lidar observations with aerosol modelling

Y. Wang et al.

Title Page

Abstract	Introduction
Conclusions	References
Tables	Figures

|◄ | ►|

◄ | ►

Back | Close

Full Screen / Esc

Printer-friendly Version

Interactive Discussion

Full Screen / Esc

Printer-friendly Version

Interactive Discussion

Abstract

In this study, we investigate the ability of the chemistry transport model (CTM) PO-LAIR3D of the air quality modelling platform POLYPHEMUS of simulating lidar backscat-tered profiles from model aerosol concentration outputs. To do so, simulated lidar signals are compared to hourly lidar observations performed during the MEGAPOLI (Megacities: Emissions, urban, regional and Global Atmospheric POLlution and cli-mate effects, and Integrated tools for assessment and mitigation) summer experiment in July 2009, where a ground-based mobile lidar was deployed around Paris on-board a van. The comparison is performed for six different measurement days, 1, 4, 16, 21, 26 and 29 July 2009, corresponding to different levels of pollution and different at-mospheric conditions. POLYPHEMUS correctly reproduces the vertical distribution of aerosol optical properties and their temporal variability. In the second part of this study, two new algorithms for assimilating lidar observations are presented. The aerosol simulations without and with lidar data assimilation are evaluated using the Airparif (a regional operational network in charge of air quality survey around the Paris area) database to demonstrate the feasibility and the usefulness of assimilating lidar profiles for aerosol forecasts.

1 Introduction

Aerosols are key air quality species to monitor and model as they impact vegetation and as they impact human health by penetrating the respiratory system and leading to respiratory and cardiovascular diseases (Lauwerys et al., 2007; Dockery and Pope, 1996). They also impact visibility (Wang et al., 2009), and they represent an uncertain component of climate changes due to their effects on the Earth's radiative budgets (In-tergovernment Panel on Climate Control, IPCC). In air quality, in order to simulate and predict particle concentrations, modellers have developed various chemistry transport models (CTM) in the past several years, e.g. EMEP (European Monitoring and Eval-

uation Programme) (Simpson et al., 2003), LOTOS (Long Term Ozone Simulation) – EUROS (European Operational Smog) (Schaap et al., 2004), CHIMERE (Hodzic et al., 2006), DEHM (Danish Eulerean Hemispheric Model) (Brandt et al., 2007) and POLYPHEMUS (Sartelet et al., 2007). However, the aerosol vertical distribution is poorly quantified, because of numerous uncertainties on aerosol sources (direct emissions) and on processes affecting aerosol formation, e.g. nucleation, condensation, evaporation, and coagulation, as well as on meteorological conditions. As the aerosol lifetime ranges from 1 to 10 days (Seinfeld and Pandis, 1998), improvements in the representation of their vertical distribution may lead to improved surface concentrations (lower error and higher correlation against observations) (Wang et al., 2013).

Various measurement types have been used to evaluate models. The most frequently used data are in situ surface measurements, e.g. AirBase (http://www.eea.europa.eu/) and EMEP over Europe, BDQA (Base de Données de la Qualité de l'Air) (Sartelet et al., 2007; Konovalov et al., 2009). However, they do not provide direct information on vertical profiles.

Satellite passive remote sensors (e.g. the Moderate Resolution Imaging Spectro-radiometers, MODIS) and sun-photometer surface stations (e.g. the AErosol RObotic NETwork, AERONET) have greatly enhanced our ability to evaluate models. Comparisons between observed and simulated Aerosol Optical Depth (AOD) have been implemented for global models and regional models (Kinne et al., 2006; Tombette et al., 2008; Péré et al., 2010). However, instruments, such as sun photometers can only retrieve column-integrated aerosol properties and can only work during the daytime.

As accurate vertical profiles of aerosols can be measured by aerosol lidars, lidar measurements were used in several campaigns, for example to evaluate the transport of particles (Chazette et al., 2012). Moreover, aerosol lidar networks, such as the European Aerosol Research Lidar Network (EARLINET), are being developed at in situ sites. In space, measurements are performed with the Cloud-Aerosol Lidar with Orthogonal Polarisation (CALIOP) lidar (Winker et al., 2007). Lidar measurements have been used for the validation of aerosol models. For example, Hodzic et al. (2004) com-

Comparison of lidar observations with aerosol modelling

Y. Wang et al.

Title Page

Abstract	Introduction
Conclusions	References
Tables	Figures

|◄ | ►|

◄ | ►

Back | Close

Full Screen / Esc

Printer-friendly Version

Interactive Discussion

pared vertical profiles simulated by CHIMERE with those observed by lidars, from EARLINET, and Stromatas et al. (2012) used observations from the CALIOP space-based lidar. Royer et al. (2011) used an optical-to-mass relationships (urban, pre-urban and rural) to retrieve the PM_{10} (particulate matter with diameter less than 10 μm)

5 concentrations from lidar signals (Raut et al., 2009a, b). In Royer et al. (2011), lidar-derived PM_{10} concentrations were compared with simulations from POLYPHEMUS and CHIMERE during the MEGAPOLI (Megacities: Emissions, urban, regional and Global Atmospheric POLlution and climate effects, and Integrated tools for assessment and mitigation) summer experiment in July 2009.

10 This paper is devoting to evaluating the lidar signal simulated by POLYPHEMUS during the MEGAPOLI summer experiment, when a ground-based mobile lidar (GBLM) was deployed around Paris on-board a van. Measurements from a ground-based in situ lidar at Saclay were also performed on 1 July 2009. This evaluation can also be regarded as a preprocessing stage of data assimilation (validation of the observation

15 operator).

Data assimilation (DA hereafter) can reduce the uncertainties in input data such as initial or boundary conditions by coupling models to observations (Bouttier and Courtier, 2002). In air quality, applications of DA to PM_{10} forecast using in situ surface measurements have been performed by Denby et al. (2008) and Tombette et al.

20 (2009) over Europe, and Pagowski et al. (2010); Pagowski and Grell (2012); Li et al. (2013) over the United States of America. Over Europe, the efficiency of assimilating lidar measurements to improve PM_{10} forecast has been compared to the efficiency of assimilating in situ surface measurements by Wang et al. (2013). They suggested that the assimilation of lidar observations may be more efficient to improve PM_{10} fore-

25 cast, although it depends on the number of lidar stations used. However, Wang et al. (2013) did not directly assimilate the lidar signal, but they used a relation between mass concentration and optical properties of pollution aerosol. Although this kind of relation has been determined for pollution aerosols over Greater Paris (Raut et al., 2009a), it needs to be generalised to other measurement sites before operationally assimilating

the mass concentration converted from the lidar signal. Moreover, the uncertainly linked to the estimation of mass concentrations may be about 25 % (Raut et al., 2009a). It is mostly due to uncertainties in estimating the specific cross sections. Because uncertainties in the lidar signal may be less than 5 %, it is more accurate to directly assimilate
5 lidar signals.

This paper is organised as follows. Section 2 describes the experiment setup, i.e. the chemistry transport model used (POLYPHEMUS) and the observations. In Sect. 3, the lidar observation operator is presented. Section 4 describes the evaluation of the simulation with in situ surface measurements and AERONET data. Results of the com-
10 parisons between observed and simulated lidar signals are shown in Sect. 5. A new algorithm for the assimilation of lidar observations and results are shown in Sect. 6. The findings are summarised and discussed in Sect. 7.

2   Experiment setup

2.1   Presentation of the model

15 In this study, the POLAIR3D air quality model (Sartelet et al., 2007) of the air quality platform POLYPHEMUS, available at http://cerea.enpc.fr/polyphemus/ and described in Mallet et al. (2007), is used to simulate air quality over the Greater Paris area. Aerosols are modelled using the SIze-REsolved Aerosol Model (SIREAM-SuperSorgam), which is described in Debry et al. (2007) and Kim et al. (2011). SIREAM-SuperSorgam in-
20 cludes 20 aerosol species: 3 primary species (mineral dust, black carbon and primary organic species), 5 inorganic species (ammonium, sulfate, nitrate, chloride and sodium) and 12 organic species. Five bins logarithmically distributed over the size range 0.01– 10 μm are used. The chemical mechanism CB05 (Carbon Bond version 5) is used for the gas chemistry (Yarwood et al., 2005). POLAIR3D/SIREAM has been used for sev-
25 eral applications. For example, it was compared to in situ surface measurements for gas and aerosols over Europe by Sartelet et al. (2007, 2012); Couvidat et al. (2012),

over Greater Paris by Couvidat et al. (2013), it was compared to AERONET data over Europe by Tombette et al. (2008) and to satellite data by Zhang et al. (2013), and it was compared to lidar-derived PM_{10} mass concentrations over Greater Paris during MEGAPOLI by Royer et al. (2011).

2.2 Modelling setup and observational data

The modelling domain is the same as the one used in Royer et al. (2011); Couvidat et al. (2013). It covers the Greater Paris area ([1.2° E, 3.5° E] × [47.9° N, 50.1° N]) with a horizontal resolution of 0.02° × 0.02°. Because Royer et al. (2011) show that limited vertical model resolution leads to much smoother vertical profiles than those deduced from lidar signals, a finer vertical resolution is used with twenty three vertical levels from the ground to 12 000 m, instead of nine vertical levels in Royer et al. (2011). The simulations are carried out for one month from 28 June to 30 July 2009. Meteorological inputs are the same as in Couvidat et al. (2013). They are simulated with the Weather Research and Forecasting (WRF) model (Skamarock et al., 2008) using an urban canopy model and an undated Corine land-use data base (Kim, 2011) with the YSU parameterisation (Hong et al., 2006) for the planetary boundary layer (PBL) dynamics. Anthropogenic emissions of gases and aerosols are generated with the Airparif (the Paris air quality agency) inventory for the year 2005. Boundary conditions for gaseous and particulate species were obtained from nested simulations over Europe and France, presented by Couvidat et al. (2013).

The ground-based mobile lidar (GBML) used during the MEGAPOLI campaign is based on an ALS450 lidar commercialised by the LEOSPHERE company and initially developed by the Commissariat à l'Energie Atomique (CEA) and the Centre National de la Recherche Scientifique (CNRS) (Chazette et al., 2007). It provides lidar measurements at 355 nm. The main characteristics of this lidar are detailed in Royer et al. (2011). This system is particularly well-adapted to air pollution and tropospheric aerosol studies thanks to its full overlap reached at about 150–200 m height and its high vertical resolution of 1.5 m. Measurement days of 1, 4, 16, 21, 26 and 29

July 2009, which correspond to different levels of pollution from Airparif (low, moderate or high), are used for comparisons to the lidar signal. Moreover, ground-based in situ lidar measurements were performed at Saclay on 1 July 2009 from 06:49 to 16:44 UTC 1 July 2009 (the blue square in Fig. 1). These measurements are used for both the comparison and the assimilation of lidar observations.

Airparif is the regional operational network in charge of air quality survey around the Paris area. It provides hourly gases and/or aerosol (PM_{10} and $PM_{2.5}$) concentration measurements. Figure 1 shows the location of the Airparif stations with red squares and/or the magenta triangles. There are 17 stations at which PM_{10} and/or $PM_{2.5}$ concentration measurements are performed.

The AERONET (AErosol RObotic NETwork) program is a federation of ground-based remote sensing aerosol networks established by NASA and PHOTONS (Univ. of Lille 1, CNES, and CNRS-INSU), which provides a long-term, continuous and readily accessible public domain database of aerosol optical measurements performed by sun-photometers. Sun-photometers measure AOD at different wavelengths ranging from 340 to 1024 nm. AOD data are computed for three data quality levels: Level 1.0 (un-screened), Level 1.5 (cloud-screened), and Level 2.0 (cloud-screened and quality-assured). The uncertainty of AOD measurements is less than 0.02 (Holben et al., 2001). For this study, there are 2 available stations over Greater Paris: Paris (urban station) and Palaiseau (suburban station) (the green discs in Fig. 1). In this paper, Level 2.0 AOD data at 340 and 380 nm are used to derive AOD data at 355 nm following the Ångström law:

$$AOD(355) = AOD(340) \left(\frac{355}{340} \right)^{-\alpha}, \tag{1}$$

where α is the angström exponent defined by

$$\alpha = \ln \left(\frac{AOD(340)}{AOD(380)} \right) \bigg/ \ln \left(\frac{380}{340} \right). \tag{2}$$

3 Methodology

This section presents the methodology used in POLYPHEMUS to derive the lidar observation operator. The range-corrected lidar signal PR_2 measured at an altitude z is defined by Collis and Russell (1976)

$$PR_2(z) = C(\beta_m(z) + \beta_a(z)) \exp\left(-2\int_0^z (\alpha_m(z') + \alpha_a(z'))dz'\right), \tag{3}$$

where β_m (resp. β_a) is the molecular (resp. aerosol) backscatter coefficient, α_m (resp. α_a) is the molecular (resp. aerosol) extinction coefficient, and C is the instrumental constant for each channel depending on the technical characteristics of the emitting and receiving optics. In order to eliminate the instrumental constant C (because it is unknown), PR_2 is normalised as follows

$$H(z) = \frac{PR_2(z)}{PR_2(z_{ref})} = \frac{\beta_m(z) + \beta_a(z)}{\beta_m(z_{ref}) + \beta_a(z_{ref})} \exp\left(2\int_z^{z_{ref}} (\alpha_m(z') + \alpha_a(z'))dz'\right), \tag{4}$$

where z_{ref} is taken at an altitude in the molecular zone. In Eq. (4), to estimate the normalised lidar signal H, four optical parameters β_m, β_a, α_m and α_a are needed.

The molecular backscatter coefficient (β_m) at the wavelength λ of the incident light is calculated by Nicolet (1984)

$$\beta_m = \frac{P}{k_B T} \cdot s_{Ray}, \tag{5}$$

where P is the pressure, T is the temperature, k_B is the Boltzmann constant, and the Rayleigh scattering cross section s_{Ray} is given by

$$s_{Ray} = 4.678 \times 10^{-29} \cdot \lambda^{-(3.916 + 0.074 \cdot \lambda + 0.05/\lambda)}. \tag{6}$$

Full Screen / Esc

Printer-friendly Version

Interactive Discussion

The molecular extinction coefficient (α_m) is given by Nicolet (1984)

$$\alpha_m = \frac{8\pi}{3}\beta_m. \tag{7}$$

Aerosol backscatter and extinction coefficients (β_a and α_a) are functions of particle sizes, of the aerosol complex refractive index (ACRI) of particles m, and of the wavelength λ of the incident light. With a population of different-sized particles of identical refractive index m and with a number size distribution function $n(D_{wet})$ with D_{wet} the particle wet diameter, the aerosol extinction and backscatter coefficients are given by the following formulas:

$$\alpha_a = \int_0^{D_{wet}^{max}} \frac{\pi D_{wet}^2}{4} Q_{ext}(m, a_{wet}) n(D_{wet}) dD_{wet}, \tag{8}$$

and

$$\beta_a = \int_0^{D_{wet}^{max}} \frac{\pi D_{wet}^2}{4} Q_{bsca}(m, a_{wet}) n(D_{wet}) dD_{wet}, \tag{9}$$

where D_{wet}^{max} is a wet diameter upper limit for the particle population, $a_{wet} = \frac{\pi D_{wet}}{\lambda}$ a dimensionless size parameter, $Q_{ext}(m, a_{wet})$ and $Q_{bsca}(m, a_{wet})$ are extinction and backscatter efficiencies. These efficiencies are computed through the Mie code (de Rooij and van der Stap, 1984; Mishchenko et al., 2002) from ftp://ftp.giss.nasa.gov/pub/crmim/spher.f. The dry complex refractive index (CRI) is interpolated from the OPAC package (Hess et al., 1998) for each species at the desired wavelength λ (355 nm). The CRI and densities used for calculation of optical properties are shown in Table 1. The wet diameter D_{wet} is computed from the mean dry diameter of each section of the aerosol sectional model SIREAM and from the aerosol water

Comparison of lidar observations with aerosol modelling

Y. Wang et al.

Title Page

Abstract	Introduction
Conclusions	References
Tables	Figures

◄ ►

◄ ►

Back Close

Full Screen / Esc

Printer-friendly Version

Interactive Discussion

content. The aerosol water content is calculated from the thermodynamic model ISOR-ROPIA (Nenes et al., 1998).

Computing the ACRI requires to make an assumption on the mixing state of the aerosol chemical species. The current version of POLYPHEMUS is based on an assumption of aerosol internal mixing: all the particles of a given size section at a given grid point of the domain are supposed to have the same chemical composition. Within this framework, Tombette et al. (2008) compared aerosol optical properties using 2 different assumptions for the Black Carbon (BC) mixing state: internally homogeneous mixing and core-shell mixing. In the internally homogeneous mixing case, BC is treated as the other components and a volume-weighted ACRI is calculated from the CRI of pure species. In the core-shell mixing case, each particle is assumed to have a structure: the core (BC) and the shell (all the other components). The hypothesis of an internally homogeneous mixing state seems to be unphysical as BC can not be well-mixed in the particle because of its complex geometry and solid state (Katrinak et al., 1993; Sachdeva and Attri, 2007). Tombette et al. (2008) have shown that the use of these two mixing states leads to negligible differences on AOD, but non-negligible differences on single scattering albedo and absorption process, in agreement with illustrations of Jacobson (2000). Thus, a core-shell mixing hypothesis is used in this study. The Maxwell-Garnett approximation is used to calculate ACRI from the core CRI (i.e., BC in this study) and the shell CRI (where all the other components are well mixed).

3.1 Estimation of z_{ref}

The altitude used to normalise the lidar signal does not need to correspond exactly to the beginning altitude of the molecular zone, but it could be any arbitrary chosen altitude in the molecular zone, where there is almost no aerosol. However, it is better to use an estimation of the normalisation altitude as close as possible to the beginning of the molecular zone, because lidar signals are attached to higher uncertainties at high altitudes. Although the molecular zone is often determined visually from lidar vertical profiles, this method is not efficient to treat large amounts of lidar profiles. We therefore

created a new algorithm which can automatically estimate the normalisation altitude z_{ref} from the lidar vertical profile.

The normalisation altitude z_{ref} is estimated from the lidar signal and the simulated molecular signal S_{Ray}

$$S_{Ray}(z) = \beta_m(z)\exp\left(-2\int_0^z \alpha_m(z')dz'\right), \tag{10}$$

as follows:

– Define a weight for each vertical point of the lidar signal (the vertical resolution is 1.5 m). The weights should be larger for the points that are more likely to be in the molecular zone, i.e. at high altitudes. We used $w(h) = \exp((h - h_{max})/L)/L$, where h is the altitude of the points, h_{max} is the maximal altitude considered (e.g. 4 km) and the parameter L is taken equal to 200 m.

– Fit all lidar signal vertical points (noted as a vector $\boldsymbol{y}$) with a weighted least absolute deviations (LAD) regression (DasGupta and Mishra, 2007). In detail, we minimise

$$\|(\boldsymbol{y} - (a\boldsymbol{h} + b))^T\boldsymbol{w}\|_{L1} = \sum_i |w_i(y_i - ah_i - b)| \tag{11}$$

to find a and b (cyan lines in Fig. 2).

– Calibrate the simulated molecular signal S_{Ray} with the LAD regression line at altitude h_{max}, and calculate the difference between the calibrated S_{Ray} and the LAD regression line at each vertical point of the lidar signal in a loop starting from high altitudes to low altitudes. The altitude at which the difference becomes larger than a pre-assigned value (1 % of the value corresponding to the LAD regression line) corresponds to z_{ref}.

Figure 2 shows comparisons between the lidar signal and the simulated molecular signal S_{Ray} for different lidar measurement days during MEGAPOLI. The simulated molecular signal (red lines in Fig. 2) agrees well with the lidar observations (blue points in Fig. 2) at high altitudes in the molecular zone, leading to the determination of the molecular zone and z_{ref}.

4 Model evaluation

To evaluate air quality models, Boylan and Russell (2006) recommended PM model performance goal and criterion that are based upon an analysis of numerous PM and visibility modelling studies. The PM model performance goal corresponds to the level of accuracy that is considered to be close to the best a model can be expected to achieve. The PM model performance criterion corresponds to the level of accuracy that is considered to be acceptable for modelling applications. The Mean Fractional Bias (MFB) and the Mean Fractional Error (MFE) are proposed to evaluate model performances against observations. RMSE and correlation are also often used in the aerosol modelling community. The statistical indicators are defined in appendix A.

4.1 Model evaluation with Airparif data

Table 2 shows statistics for the month of simulation and for the 6 lidar measurement days. For the month of simulation, for $PM_{2.5}$, the MFB and MFE are respectively in the range [−30 %, 30 %] and [0, 50 %], i.e. the PM model performance goal is met. For PM_{10}, the MFB and MFE are respectively in the range [−60 %, 60 %] and [0, 75 %], i.e. the PM model performance criterion is met. For each lidar measurement day, the PM model performance goal is always met for $PM_{2.5}$, and the PM model performance criterion is met for PM_{10} except for 29 July.

As shown in Table 2, the model simulates well $PM_{2.5}$ concentrations, but PM_{10} concentrations are underestimated. In other words, coarse particles (particulate matter

Comparison of lidar observations with aerosol modelling

Y. Wang et al.

Title Page

Abstract	Introduction
Conclusions	References
Tables	Figures

|◄   ►|

◄   ►

| Back | Close |

Full Screen / Esc

Printer-friendly Version

Interactive Discussion

with a diameter higher than 2.5 µm and lower than 10 µm) are underestimated. This may be because emissions and boundary conditions of coarse particles are underestimated, e.g. road resuspensions of PM are not considered in the model and boundary conditions are obtained from nested simulations over Europe and France where coarse particles were underestimated.

4.2 Model evaluation with AERONET data

Table 3 presents statistics for hourly data: the simulation underestimates the AOD, in agreement with the result of the comparisons between the simulation and Airparif observations (see Sect. 4.1). The simulated and the observed AOD agree well on 1, 4, 16 and 26 July 2009, according to the criteria of Boylan and Russell (2006). However, the correlation is only -8% on 1 July, which is a day of high pollution (see Table 2). To understand why the correlation is low on 1 July, Fig. 3 presents the hourly evolution of the PM_{10} concentration (resp. simulated AOD) against Airparif (resp. AERONET) surface measurements at the station "Paris". On the surface, there is a good agreement (90.38 % correlation) between the simulation and Airparif observations for the PM_{10} concentration on 1 July 2009. However, the hourly simulated AOD and the surface measured PM_{10} do not correlate well with AERONET data at this station. Although the surface PM_{10} concentration starts to increase from 02:00 UTC, the AOD only begins to increase from 09:00 UTC. It means that between 02:00 and 09:00 UTC, PM_{10} concentrations are high near the surface but not at high altitudes. However, in the model, the AOD increases from as early as 05:00 UTC. A possible explanation of the discrepancy between observed and simulated AOD is that the particles are mixed by turbulence more effectively and earlier in the model than in the true state of the atmosphere on 1 July (Wang et al., 2013). As shown in Fig. 3, there is a time difference (about 2 h) between the peak of AOD and the peak of simulated/measured surface PM_{10} concentrations, probably because a strong thermic mixing occurring in the late morning during this lidar measurement day (Royer et al., 2011).

5 Comparisons with lidar vertical profiles

The simulated lidar signal is compared with GBML observations performed during the MEGAPOLI summer experiment on the different measurements days (1, 4, 16, 21, 26 and 29 July 2009). The purpose of this section is to validate the ability of POLYPHEMUS to simulate lidar backscattered profiles and then choose suitable measurement days to do assimilation tests.

On 1 July 2009, GBML measurements are performed leeward inside the pollution plume in the Southwest of Paris between Saclay and Chateaudun during 3 h (the black track in Fig. 1). It is the most polluted day of the MEGAPOLI experiment. High levels of PM_{10}, on average about $45\,\mu g\,m^{-3}$ (see Table 2), are measured by the Airparif network. Figure 4 presents the comparison between lidar observations and the simulation at 11:00, 12:00 and 13:00 UTC. It shows that POLYPHEMUS underestimates the lidar signal at 13:00 UTC, but it overestimates it at 14:00 UTC and it agrees well with observations at 15:00 UTC. While the boundary layer height increases from about 1.2 to 1.8 km from 11:00 to 13:00 UTC and the GBML runs out of the pollution plume (Royer et al., 2011), both the observed and simulated lidar signals decrease. Figures of the comparison between the simulation and observations from a ground-based in situ lidar at Saclay are shown later in this paper (see Fig. 11). The pollution plume covers Saclay because of the northeast wind. Thus high lidar signal values in both the simulation and observations are seen after 10:00 UTC, although the simulated lidar signals are underestimated. Data assimilation (DA) will be performed for this day, as it is the most polluted day with observations from both the GMBL and a ground-based in situ lidar.

On 4 July 2009, GBML measurements are performed around Paris with a circular pattern from 14:49 to 17:24 UTC. Particle AOD and concentrations are underestimated in the simulation. The daily averaged AOD from the AERONET network is about 0.25, respectively 0.14 in the simulation (see Table 3). The daily averaged PM_{10} concentration from the Airparif network is about $18.37\,\mu g\,m^{-3}$, respectively $11.11\,\mu g\,m^{-3}$ in the simulation (see Table 2). Figure 5 shows comparisons between the GBML measure-

ments and the simulation at 15:03 UTC and 16:00 UTC. The simulated lidar signals are underestimated. Moreover, lidar measurements show an aerosol layer between 2.0 km and 3.0 km (probably from long-range transport), which is not present in the simulation.

On 16 July 2009, GBML measurements are performed in the North of Paris from Saclay to Amiens between 11:00 UTC and 14:30 UTC. The lidar signal is overall underestimated, as shown in Fig. 6, in agreement with the underestimation of PM_{10} shown by the statistics in Tables 2 and 3. Surface PM_{10} concentration from the Airparif network and from the simulation are respectively 26.25 and 16.47 µg m^{-3} (low-moderate level of pollution, see Table 2). The observed and simulated AOD are respectively 0.26 and 0.18 (see Table 3). The simulated AOD has a good correlation with AERONET data (up to 80 %). As deduced from the comparisons of the modelled and observed lidar signals in Fig. 6, the PBL height is well modelled until 12:00 UTC, but it is underestimated afterwards, e.g. the PBL height is about 2.1 km from the observed lidar signal but it is about 1.6 km in the simulation. These differences in PBL height explain that the simulated lidar signal agrees better with the observation until 12:00 UTC.

On 21 July 2009, the GBML travels from Saclay to the North of Paris across the city centre of Paris. As shown in Fig. 7, the lidar signal is overestimated for this measurement day. However, the surface PM_{10} concentration is underestimated. It is 27.84 and 16.84 µg m^{-3} (low-moderate level of pollution, see Table 2) from the Airparif network and from the simulation respectively. The large simulated lidar signals originate in high aerosol concentration at high altitudes, i.e. between 2.0 km and 2.5 km, which leads to higher backscatter and extinction coefficients. This high-altitude aerosol layer originates in boundary conditions, but it is not present in the observations. It impacts the lidar signal until low altitudes. This is why surface PM_{10} is underestimated while lidar signal is overestimated.

On 26 July 2009, the GBML followed two circular patterns (the yellow and cyan tracks in Fig. 1). One is performed from 12:40 to 15:30 UTC at a distance between 15 and 30 km from the city centre. Another one is performed from 16:44 to 18:18 UTC in the south-southwest of Paris. Low levels of pollution are observed and simulated.

Title Page

Abstract | Introduction

Conclusions | References

Tables | Figures

|◄ | ►|

◄ | ►

Back | Close

Full Screen / Esc

Printer-friendly Version

Interactive Discussion

Surface PM_{10} concentrations and AOD are underestimated. The daily averaged PM_{10} concentration from Airparif is $18.04\,\mu g\,m^{-3}$, against $10.12\,\mu g\,m^{-3}$ in the simulation. The mean observed AOD value is 0.15, against 0.08 in the simulation. Although the lidar signal is slightly underestimated in the simulation, simulated and observed lidar signals agree fairly well, as shown in Fig. 8. The pollution from Paris is transported by the south wind to the north. This is why the lidar signal is higher at 14:00 UTC in Fig. 8. Because as much as 5 h of lidar measurements are performed, which is longer than on 4, 16, 21 and 29 July 2009, we will perform DA for this day.

On 29 July 2009, GBML measurements are performed from 12:22 to 15:10 UTC in the North of Paris and in peri-urban and rural areas. While low levels of pollution ($12.33\,\mu g\,m^{-3}$ of the mean PM_{10} concentration in Table 2) are simulated, moderate levels of pollution ($29.25\,\mu g\,m^{-3}$ of the mean PM_{10} concentration in Table 2) are observed by the Airparif network. As deduced from Fig. 9, at the beginning of measurement period, the PBL height is about 1.5 km and the simulated lidar signal agrees well with lidar observations. At 15:00 UTC, the observed lidar signal has increased, because of an aerosol layer between 2.0 and 3.5 km. This layer is not simulated and the simulated lidar signal is underestimated.

6 Assimilation test of lidar observations

As mentioned in the previous section of comparisons between the simulation and the lidar observations during the MEGAPOLI summer experiment in July 2009, DA run is performed for 1 (13 h of measurements) and 26 (5 h of measurements) July 2009.

In air quality, the large number of state variables leads to high computational costs when implementing DA algorithms. Among the widely used DA algorithms, the optimal interpolation (OI) is used here, as it is the most computationally efficient (Denby et al., 2008; Tombette et al., 2008; Wu et al., 2008; Li et al., 2013). In applications of DA to aerosol forecasts, Tombette et al. (2009) have used the OI over western Europe for assimilating observations from the BDQA network, which covers France. Denby et al.

(2008) have used two different DA techniques, the OI and EnKF, to assimilate PM_{10} concentrations over Europe. Pagowski et al. (2010) have used the OI over the United States of America for data assimilation of $PM_{2.5}$ observations. Li et al. (2013) have used the OI for multiple aerosol species and for prediction of $PM_{2.5}$ in the Los Angeles basin. And Wang et al. (2013) have used the OI over Europe to investigate the potential impact of future ground-based lidar networks on analysis and short-term forecasts of PM_{10}.

6.1 Basic formulation

The basic formulation of DA of lidar signals with OI is now described. Particles are represented in the model by mass concentrations of different chemical species for the different particle size sections.

The state vector x is defined by

$$x = \left\{ x_{i,j,k}^{h} \right\}_{1 \leq i \leq N_{b}, 1 \leq j \leq N_{s}, 1 \leq k \leq n, 1 \leq h \leq l}, \tag{12}$$

where $x_{i,j,k}^{h}$ is the mass concentration of the aerosol species j in section i for the horizontal spatial grid k at the model vertical level h, N_{b} is the number of size sections, N_{s} is the number of chemical species, n is the number of horizontal grid points at each vertical level h and l is the total number of vertical levels. The lidar observation operator is $H(x) = \mathbf{L} \cdot S(x)$, where S is a nonlinear operator from the model state x to the lidar signal state, and $\mathbf{L}$ is a linear spatial interpolation operator.

The analysed state vector is a solution to the variational optimisation problem:

$$x^{a} = \text{Argmin} \quad J(x), \tag{13}$$

where J is the cost function defined by

$$J(x) = \frac{1}{2}(H(x) - y^T R^{-1}(H(x) - y) + \frac{1}{2}(x - x^b)^T B^{-1}(x - x^b)$$

$$\simeq \frac{1}{2}(H(x^b) + LS(x - x^b) - y)^T R^{-1}(H(x^b) + LS(x - x^b) - y)$$

$$+ \frac{1}{2}(x - x^b)^T B^{-1}(x - x^b), \tag{14}$$

where **S** is the tangent linear of operator S, **B** and **R** are the matrices of error covariances for backgrounds and observations respectively, and y is the vector of observations. In this way, we have

$$\nabla J(x^a) = (LS)^T R^{-1}(H(x^b) - y) + (B^{-1} + (LS)^T R^{-1}(LS))(x^a - x^b) = 0, \tag{15}$$

which leads to

$$x^a - x^b = (B^{-1} + (LS)^T R^{-1}(LS))^{-1}(y - H(x^b)) \tag{16}$$

$$= B(LS)^T((LS)B(LS)^T + R)^{-1}(y - H(x^b)). \tag{17}$$

6.2 Construction of error covariances

As the measurements at different levels originate from the same lidar, the matrix **R** should not be diagonal because of measurement error correlations. However, in order to simplify **R** in the first tests of DA of lidar observations, one takes $R = rI$ as a diagonal matrix where **I** is the identity matrix and r is an error variance. The value of the observation error variance r is determined by a χ^2 diagnosis (Ménard et al., 1999), in which the scalar

$$\chi^2 = (y - H(x^b))^T((LS)B(LS)^T + R)^{-1}(y - H(x^b)) \tag{18}$$

should be equal, on average, to the number of observations (N) at each DA step.

Specifically, **B** plays a role in determining how the corrections of concentrations should be distributed over the domain during DA. In practice, however, it is impossible to accurately know all coefficients of **B**. In our simulation, the number of model grid points is of the order of 10^5. Thus the number of coefficients in the matrix **B** is about 10^{10} multiplied by the square of the number of analysis variables (about 100 variables for particles are used here). Therefore, **B** is too large to be handled numerically.

In order to reduce the size of the error covariance matrix for background, i.e. **B**, we model the matrix **B** as follows

$$\mathbf{B} = \mathbf{PDP}^{\mathsf{T}}, \tag{19}$$

where **D** is the error covariance matrix for PM_{10}, defined by the Balgovind approach (Balgovind et al., 1983) obtained by considering the RMSE and correlation of simulated PM_{10} concentrations. Thus, the size of **D** is much less than the one of **B**. The matrix **P** is defined by

$$\mathbf{P} = \begin{bmatrix} \boldsymbol{v}_1 & \mathbf{0} & \dots & \mathbf{0} \\ \mathbf{0} & \boldsymbol{v}_2 & \dots & \mathbf{0} \\ \vdots & \vdots & \ddots & \vdots \\ \mathbf{0} & \mathbf{0} & \dots & \boldsymbol{v}_M \end{bmatrix}_{(M \cdot N_b \cdot N_s) \times M},$$

where M is equal to the dimension of the domain ($l \cdot n$), $\boldsymbol{v}_k$ is a vector of size $N_b \cdot N_s$ (the number of state variables). Each component of $\boldsymbol{v}_k$ corresponds to the proportion of the mass of particles for a given species in a given size section in PM_{10} mass concentrations at grid point k.

Let $\mathbf{S}' = \mathbf{SP}$ be the directional derivative of S along a given direction, and let $\boldsymbol{c}^b$ and $\boldsymbol{c}^a$ be PM_{10} concentration states before and after analysis respectively. We multiply

Title Page

Abstract | Introduction

Conclusions | References

Tables | Figures

|◀ | ▶|

◀ | ▶

Back | Close

Full Screen / Esc

Printer-friendly Version

Interactive Discussion

each side of Eq. (17) by the matrix $\mathbf{Z}$ in order to convert $\boldsymbol{x}$ into the PM_{10} state $\boldsymbol{c}$:

$$\mathbf{Z} = \begin{bmatrix} 1\ldots1 & 0\ldots0 & 0\ldots0 & 0\ldots0 \\ 0\ldots0 & 1\ldots1 & 0\ldots0 & 0\ldots0 \\ \vdots\ddots\vdots & \vdots\ddots\vdots & \vdots\ddots\vdots & \vdots\ddots\vdots \\ 0\ldots0 & 0\ldots0 & 0\ldots0 & 1\ldots1 \end{bmatrix}_{M\times(M\cdot N_b\cdot N_s)} .$$

We obtain

$$\boldsymbol{c}^a - \boldsymbol{c}^b = \mathbf{D}(\mathbf{LS}')^{\mathsf{T}}\left((\mathbf{LS}')\mathbf{D}(\mathbf{LS}')^t + \mathbf{R}\right)^{-1}(\boldsymbol{y} - H(\boldsymbol{x}^b)). \tag{20}$$

After the analysis, the concentrations $\boldsymbol{c}^a$ are redistributed over particle species and size sections following the initial chemical and size distributions.

6.3 DA setup

DA experiments are carried out for 1 and 26 July 2009. All DA experiments are performed with time step 600 s and from 200 to 1800 m above the ground (10 model levels), since lidar measurements are not available below the altitude of full overlap (200 m above the ground) and since aerosol concentrations above the PBL have limited impact on surface PM_{10} in the short term (Wang et al., 2013). In the Balgovind approach, the horizontal correlation length is set to 0.2°, which is estimated from numerical DA tests. The error variances are separately set for each DA level, depending on the RMSE of PM concentrations and the variability of PM concentrations at each model level.

Two new algorithms are tested for the assimilation of lidar observations. In the first algorithm, we use the assimilation of lidar observations to analyse PM_{10} concentrations and the analysed PM_{10} concentrations are redistributed over particle species and size sections following the initial chemical and size distributions (see Sect. 6.2). The background error variances (PM_{10}) are estimated by the simulation without DA and Airparif observations. The value of the observation error variance r is determined by a χ^2

Full Screen / Esc

Printer-friendly Version

Interactive Discussion

diagnosis, which yields $r = 1\,\mu g^2\,m^{-6}$ and $r = 0.006\,\mu g^2\,m^{-6}$ respectively for 1 and 26 July, depending on the level of uncertainties (see Sect. 5). Let N be the number of lidar observations at one DA step. Figure 10 shows time evolutions of χ^2/N (blue lines) for DA runs on 1 and 26 July. The mean over DA window of χ^2/N is 1.02 (resp. 1.02) for 1 (resp. 26) July.

In the second algorithm, we separately analyse $PM_{2.5}$ and $PM_{2.5-10}$ (particulate matter with a diameter higher than 2.5 µm and lower than 10 µm) in the assimilation of lidar observations. We modify the matrices used in Sect. 6.2 to obtain $c_{2.5}$ and $c_{2.5-10}$, the mass concentrations of $PM_{2.5}$ and $PM_{2.5-10}$ respectively (see Appendix B for details). We separately set the error variances for $PM_{2.5}$ and $PM_{2.5-10}$ in matrix **D**. Because of the lack of $PM_{2.5-10}$ observations, we can not directly estimate the background error variances. They are determined by a χ^2 diagnosis using the observation error variance r found in the first algorithm.

In the following, we note the assimilation with the first (resp. second) DA algorithm as "DA (PM_{10})" (resp. "DA ($PM_{2.5}$ and $PM_{2.5-10}$)").

6.4 Results and discussions

In these DA tests, the purpose is to verify if these new algorithms are functional. Because we work at a small scale, the corrections of DA are transported out of the simulation domain very quickly. Thus we only compute the statistics for the DA window to validate the DA tests.

Table 4 presents statistics of the simulation results without DA and with DA. Statistics are computed for both PM_{10} and $PM_{2.5}$ concentrations. Overall, both DA algorithms lead to better scores (lower RMSE, MFB and MFE, and higher correlation) than the simulation without DA for PM_{10} concentrations. Comparing two DA algorithms, the simulation with DA ($PM_{2.5}$ and $PM_{2.5-10}$) leads to better scores than the simulation with DA (PM_{10}) for PM_{10} concentrations (see Table 4). The RMSE of PM_{10} is $11.63\,\mu g\,m^{-3}$ in the simulation with DA ($PM_{2.5}$ and $PM_{2.5-10}$), against $13.69\,\mu g\,m^{-3}$ in the simulation

with DA (PM_{10}) on 1 July. The RMSE of PM_{10} is $4.73\,\mu g\,m^{-3}$ in the simulation with DA ($PM_{2.5}$ and $PM_{2.5-10}$), against $6.08\,\mu g\,m^{-3}$ in the simulation with DA (PM_{10}) on 26 July. It is because higher background error variances are set for coarse sections in the simulation with DA ($PM_{2.5}$ and $PM_{2.5-10}$). However, the simulation with DA ($PM_{2.5}$ and $PM_{2.5-10}$) leads to similar scores to the simulation with DA (PM_{10}) for $PM_{2.5}$ concentrations (see Table 4). It is because similar background error variances for $PM_{2.5}$ in the simulation with DA ($PM_{2.5}$ and $PM_{2.5-10}$) to the simulation with DA ($PM_{2.5}$) are used in the χ^2 diagnosis (fine particles contribute to more than 80 % of the lidar signal (Randriamiarisoa et al., 2006)). In the following, we compare the simulation without DA and the simulation with DA ($PM_{2.5}$ and $PM_{2.5-10}$).

On 1 July, the averaged RMSE of PM_{10} is $11.63\,\mu g\,m^{-3}$ with DA ($PM_{2.5}$ and $PM_{2.5-10}$), against $17.74\,\mu g\,m^{-3}$ without DA. The decrease of the RMSE is explained by the correlation length in the matrix **D**, since no Airparif station performs measurements in the Southwest of Paris (the Northeast wind). At station *ISSY-LES-MOULINEAUX*, the closest station to Saclay, the RMSE of PM_{10} is $14.72\,\mu g\,m^{-3}$ with DA ($PM_{2.5}$ and coarse), against $22.81\,\mu g\,m^{-3}$ without DA. However, the averaged RMSE of $PM_{2.5}$ is about $10.4\,\mu g\,m^{-3}$ with DA ($PM_{2.5}$ and $PM_{2.5-10}$), against $8.54\,\mu g\,m^{-3}$ without DA. This is due to the larger horizontal correlation length (see Sect. 6.3). Figure 11 shows that the model underestimates the lidar signal at Saclay. While DA runs increase PM concentrations in the lidar measurement grids, PM concentrations are increased at Airparif stations, where $PM_{2.5}$ concentrations is well simulated and coarse particles are underestimated. This problem can be solved by decreasing the horizontal correlation length.

On 26 July, the averaged RMSE of PM_{10} is $4.73\,\mu g\,m^{-3}$ with DA ($PM_{2.5}$ and $PM_{2.5-10}$), against $6.67\,\mu g\,m^{-3}$ without DA. Because two circular GBML travelling patterns were performed around Paris (see Fig. 1), most of Airparif stations are leeward (the South wind) or they are close to the patterns of GBML. They could validate improvements of PM concentrations. At station *PARIS 1er Les Halles*, the RMSE of PM_{10} is $1.96\,\mu g\,m^{-3}$ in the simulation with DA ($PM_{2.5}$ and $PM_{2.5-10}$), against $4.71\,\mu g\,m^{-3}$ in

the simulation without DA. Moreover, DA runs lead to better scores than the simulation without DA for $PM_{2.5}$. At leeward station *CREIL FAIENCERIE*, the RMSE of $PM_{2.5}$ is $4.1\,\mu g\,m^{-3}$ in the simulation with DA ($PM_{2.5}$ and $PM_{2.5-10}$), against $4.9\,\mu g\,m^{-3}$ in the simulation without DA.

7 Conclusions

In order to investigate the ability of the CTM POLAIR3D of the air quality modelling platform POLYPHEMUS to simulate lidar vertical profiles, we have performed a simulation in the Greater Paris area for the summer month July 2009. The results (PM_{10} and $PM_{2.5}$ concentrations) are evaluated by Airparif data. We have simulated aerosol optical properties and lidar signals from the model aerosol concentration outputs using the aerosol complex refractive index (ACRI) and the wet particle diameter. Hourly comparisons between simulated lidar signals and lidar observations have been described for six measurement days during the MEGAPOLI summer campaign. These comparisons have shown a good agreement between GBML measurements and the simulation except 21 July 2009, where an aerosol layer was presented at higher altitude in the model. The results show that the optical property module of POLYPHEMUS would reproduce correctly lidar signals in the model, if the aerosol layer is well simulated.

Two new algorithms for the assimilation of lidar observations have been presented. That depends on whether PM_{10} is analysed or $PM_{2.5}$ and $PM_{2.5-10}$ are both analysed. DA tests were performed for 1 and 26 July 2009. On the whole, both of these algorithms lead to better scores (lower RMSE, MFB and MFE, and higher correlation) for PM_{10}. However, they did not work for $PM_{2.5}$ on 1 July 2009, because of the larger horizontal correlation length. The simulation with DA ($PM_{2.5}$ and $PM_{2.5-10}$) leads to better scores than the simulation with DA (PM_{10}) by setting separately the error variances for backgrounds in fine sections and coarse sections. The results shown in this paper suggest that the assimilation of lidar observations for analysing $PM_{2.5}$ and $PM_{2.5-10}$ would

27137

perform better than assimilating the lidar signal for analysing PM_{10}, but it is computationally more costly.

Comparing the simulation without DA and the simulation with DA ($PM_{2.5}$ and $PM_{2.5-10}$), the averaged RMSE of PM_{10} is $11.63\,\mu g\,m^{-3}$ with DA ($PM_{2.5}$ and $PM_{2.5-10}$), against $17.74\,\mu g\,m^{-3}$ without DA on 1 July 2009. The averaged RMSE of PM_{10} is $4.73\,\mu g\,m^{-3}$ with DA ($PM_{2.5}$ and $PM_{2.5-10}$), against $6.67\,\mu g\,m^{-3}$ without DA on 26 July 2009.

A forthcoming paper will present results about the assimilation of continuous measurements from the ACTRIS/EARLINET network during a 72 h period of intensive observations.

Appendix A

Statistical indicators

$\{o_i\}_{i=1,n}$ and $\{s_i\}_{i=1,n}$ are the observed and the modelled concentrations at time i, respectively. n is the number of available observations. The statistical indicators used to evaluate the results with respect to observations are: the Root Mean Square Error (RMSE), the (Pearson) correlation, the Mean Fractional Error (MFE), the Mean Fractional Bias (MFB). MFE and MFB bound the maximum error and bias and do not allow a few data points to dominate the statistics. They are often used to evaluate model performances against observations for aerosol mass concentrations and optical properties

Comparison of lidar observations with aerosol modelling

Y. Wang et al.

Title Page

Abstract | Introduction

Conclusions | References

Tables | Figures

|◄ | ►|

◄ | ►

Back | Close

Full Screen / Esc

Printer-friendly Version

Interactive Discussion

(Boylan and Russell, 2006). The statistical indicators are defined as follow:

$$\text{RMSE} = \sqrt{\frac{1}{n} \sum_{i=1}^{n} (o_i - s_i)^2}, \tag{A1}$$

$$\text{correlation} = \frac{\sum_{i=1}^{n} (o_i - \overline{o})(s_i - \overline{s})}{\sqrt{\sum_{i=1}^{n} (o_i - \overline{o})^2 \sum_{i=1}^{n} (s_i - \overline{s})^2}}, \tag{A2}$$

$$\text{MFE} = \frac{1}{n} \sum_{i=1}^{n} \frac{|s_i - o_i|}{(s_i + o_i)/2}, \tag{A3}$$

$$\text{MFB} = \frac{1}{n} \sum_{i=1}^{n} \frac{s_i - o_i}{(s_i + o_i)/2}, \tag{A4}$$

where $\overline{o} = \frac{1}{n} \sum_{i=1}^{n} o_i$ and $\overline{s} = \frac{1}{n} \sum_{i=1}^{n} s_i$.

Appendix B

Update formula for DA (PM$_{2.5}$ and PM$_{2.5-10}$)

In order to separately analyse PM$_{2.5}$ and PM$_{2.5-10}$ in the assimilation of lidar observations, the matrix **B** is modelled as follows

$$\mathbf{B} = \mathbf{PDP}^{\mathrm{T}}, \tag{B1}$$

where **D** is the error covariance matrix for PM$_{2.5}$ and PM$_{2.5-10}$. The matrix **D** is defined by

$$\mathbf{D} = \begin{bmatrix} \mathbf{D}_{2.5} & \mathbf{0} \\ \mathbf{0} & \mathbf{D}_{2.5-10} \end{bmatrix}, $$

and the matrix **P** is defined by

$$\mathbf{P} = \begin{bmatrix} \mathbf{P_{2.5}} \\ \mathbf{P_{2.5-10}} \end{bmatrix},$$

where each column k of $\mathbf{P_{2.5}}$ (resp. $\mathbf{P_{2.5-10}}$) corresponds to the proportion of the mass of particles for a given species in a given size section in PM$_{2.5}$ (resp. PM$_{2.5-10}$) mass concentrations at grid point k as Sect. 6.2 shown.

The matrix **Z** is defined by

$$\mathbf{Z} = \begin{bmatrix} \mathbf{Z_{2.5}} \\ \mathbf{Z_{2.5-10}} \end{bmatrix},$$

where the matrix $\mathbf{Z_{2.5}}$ (resp. $\mathbf{Z_{2.5-10}}$) is a $M \times (M \cdot N_b \cdot N_s)$ matrix, which converts the state vector x into the PM$_{2.5}$ (resp. PM$_{2.5-10}$) state $c_{2.5}$ (resp. $c_{2.5-10}$).

Let $\mathbf{S}' = \mathbf{SP}$. After multiplying each side of Eq. (17) by the matrix **Z**, we obtain

$$\begin{pmatrix} c_{2.5}^{a} - c_{2.5}^{b} \\ c_{2.5-10}^{a} - c_{2.5-10}^{b} \end{pmatrix} = \mathbf{D}(\mathbf{LS}')^{\top}\left((\mathbf{LS}')\mathbf{D}(\mathbf{LS}')^{t} + \mathbf{R}\right)^{-1}(y - H(x^{b})).$$

The publication of this article is financed by CNRS-INSU.

Full Screen / Esc

Printer-friendly Version

Interactive Discussion

References

Balgovind, R., Dalcher, A., Ghil, M., and Kalnay, E.: A stochastic-dynamic model for the spatial structure of forecast error statistics, Mon. Weather Rev., 111, 701–722, 1983. 27133

Bouttier, F. and Courtier, P.: Data assimilation concepts and methods, Meteorological Training Course Lecture Series, ECMWF, Reading, United Kingdom, 2002. 27118

Boylan, J. W. and Russell, A. G.: PM and light extinction model performance metrics, goals, and criteria for three-dimensional air quality models, Atmos. Environ., 40, 4946–4959, 2006. 27126, 27127, 27139

Brandt, J., Christensen, J. H., Frohn, L. M., Geels, C., Hansen, K. M., Hedegaard, G. B., Hvidberg, M., and Skjøth, C. A.: THOR – an operational and integrated model system for air pollution forecasting and management from regional to local scale, in: Proceedings of the 2nd ACCENT Symposium, 2007. 27117

Chazette, P., Sanak, J., and Dulac, F.: New approach for aerosol profiling with a lidar onboard an ultralight aircraft: application to the African monsoon multidisciplinary analysis, Environ. Sci. Technol., 41, 8335–8341, 2007. 27120

Chazette, P., Bocquet, M., Royer, P., Winiarek, V., Raut, J.-C., Labazuy, P., Gouhier, M., Lardier, M., and Cariou, J.-P.: Eyjafjallajökull ash concentrations derived from both lidar and modeling, J. Geophys. Res., 117, 1–17, doi:10.1029/2011JD015755, 2012. 27117

Collis, R. T. H. and Russell, P. B.: Lidar measurements of particles and gases by elastic backscattering and differential absorption, Top. Appl. Phys., 14, 89–97, 1976. 27122

Couvidat, F., Debry, E., Sartelet, K., and Seigneur, C.: A hydrophilic/hydrophobic organic (H_2O) aerosol model: development, evaluation and sensitivity analysis, J. Geophys. Res., 117, 1–19, doi:10.1029/2011JD017214, 2012. 27119

Couvidat, F., Kim, Y., Sartelet, K., Seigneur, C., Marchand, N., Sciare, J., and Environnement, L. C.: Modeling secondary organic aerosol in an urban area: application to Paris, France, Atmos. Chem. Phys., 13, 983–996, doi:10.5194/acp-13-983-2013, 2013. 27120

DasGupta, M. and Mishra, S. K.: Least Absolute Deviation Estimation of Linear Econometric Models: a Literature Review, North-Eastern Hill University, 2007. 27125

de Rooij, W. A. and van der Stap, C. C. A. H.: Expansion of Mie scattering matrices in generalized spherical functions, Astron. Astrophys., 131, 237–248, 1984. 27123

Comparison of lidar observations with aerosol modelling

Y. Wang et al.

Title Page

Abstract	Introduction
Conclusions	References
Tables	Figures

◀ | ▶

◀ | ▶

Back | Close

Full Screen / Esc

Printer-friendly Version

Interactive Discussion

Debry, E., Fahey, K., Sartelet, K., Sportisse, B., and Tombette, M.: Technical Note: A new SIze REsolved Aerosol Model (SIREAM), Atmos. Chem. Phys., 7, 1537–1547, doi:10.5194/acp-7-1537-2007, 2007. 27119

Denby, B., Schaap, M., Segers, A., Builtjes, P., and Hora, J.: Comparison of two data assimilation methods for assessing PM_{10} exceedances on the European scale, Atmos. Environ., 42, 7122–7134, doi:10.1016/j.atmosenv.2008.05.058, 2008. 27118, 27130

Dockery, D. and Pope, A.: Epidemiology of acute health effects: summary of time-series, in: Particles in Our Air: Concentration and Health Effects, Harvard University Press, 123–147, 1996. 27116

Hess, M., Koepke, P., and Schult, I.: Optical properties of aerosols and clouds: the software package OPAC, B. Am. Meteorol. Soc., 79, 831–844, 1998. 27123

Hodzic, A., Chepfer, H., Vautard, R., Chazette, P., Beekmann, M., Bessagnet, B., Chatenet, B., Cuesta, J., Drobinski, P., Goloub, P., Haeffelin, M., and Morille, Y.: Comparison of aerosol chemistry transport model simulations with lidar and Sun photometer observations at a site near Paris, J. Geophys. Res., 109, 1–19, doi:10.1029/2004JD004735, 2004. 27117

Hodzic, A., Vautard, R., Chazette, P., Menut, L., and Bessagnet, B.: Aerosol chemical and optical properties over the Paris area within ESQUIF project, Atmos. Chem. Phys., 6, 3257–3280, doi:10.5194/acp-6-3257-2006, 2006. 27117

Holben, B. N., Tanré, D., Smirnov, A., Eck, T. F., Slutsker, I., Abuhassan, N., Newcomb, W. W., Schafer, J. S., Chatenet, B., Lavenu, F., Kaufman, Y. J., Castle, J. V., Setzer, A., Markham, B., Clark, D., Frouin, R., Halthore, R., Karneli, A., Neill, N. T. O., Pietras, C., Pinker, R. T., Voss, K., and Zibordi, G.: An emerging ground-based aerosol climatology: aerosol optical depth from AERONET, J. Geophys. Res., 106, 12067–12097, 2001. 27121

Hong, S. Y., Noh, Y., and Dudhia, J.: A new vertical diffusion package with an explicit treatment of entrainment processes, Mon. Weather Rev., 134, 2318–2341, 2006. 27120

Intergovernment Panel on Climate Control (IPCC): Climate Change 2007, the fourth Assessment Report of the IPCC, Cambridge Univ. Press, 2007. 27116

Jacobson, M. Z.: A physically-based treatment of elemental carbon optics: implications for global direct forcing of aerosols, Geophys. Res. Lett., 27, 217–220, 2000. 27124

Katrinak, K. A., Rez, P., Perkes, P. R., and Buseck, P. R.: Fractal geometry of carbonaceous agregates from an urban aerosol, Environ. Sci. Technol., 27, 539–547, 1993. 27124

Kim, Y.: Air quality modeling: evaluation of chemical and meteorological parameterizations, Ph. D. thesis, Université Paris-Est, 2011. 27120

Comparison of lidar observations with aerosol modelling

Y. Wang et al.

Title Page

Abstract	Introduction
Conclusions	References
Tables	Figures

|◄ | ►|

◄ | ►

Back | Close

Full Screen / Esc

Printer-friendly Version

Interactive Discussion

Kim, Y., Couvidat, F., Sartelet, K., and Seigneur, C.: Comparison of different gas-phase mechanisms and aerosol modules for simulating particulate matter formation, J. Air Waste Manage. Assoc., 61, 1218–1226, doi:10.1080/104732.89.2011.603939, 2011. 27119

Kinne, S., Schulz, M., Textor, C., Guibert, S., Balkanski, Y., Bauer, S. E., Berntsen, T., Berglen, T. F., Boucher, O., Chin, M., Collins, W., Dentener, F., Diehl, T., Easter, R., Feichter, J., Fillmore, D., Ghan, S., Ginoux, P., Gong, S., Grini, A., Hendricks, J., Herzog, M., Horowitz, L., Isaksen, I., Iversen, T., Kirkevåg, A., Kloster, S., Koch, D., Kristjansson, J. E., Krol, M., Lauer, A., Lamarque, J. F., Lesins, G., Liu, X., Lohmann, U., Montanaro, V., Myhre, G., Penner, J., Pitari, G., Reddy, S., Seland, O., Stier, P., Takemura, T., and Tie, X.: An AeroCom initial assessment – optical properties in aerosol component modules of global models, Atmos. Chem. Phys., 6, 1815–1834, doi:10.5194/acp-6-1815-2006, 2006. 27117

Konovalov, I. B., Beekmann, M., Meleux, F., Dutot, A., and Foret, G.: Combining deterministic and statistical approaches for PM_{10} forecasting in Europe, Atmos. Environ., 43, 6425–6434, doi:10.1016/j.atmosenv.2009.06.039, 2009. 27117

Lauwerys, R., Haufroid, V., Hoet, P., and Lison, D.: Toxicologie Industrielle et Intoxications Professionnelles, Elsevier-Masson, Issy-les-Moulineaux, France, 1252 pp., 2007. 27116

Li, Z., Zang, Z., Li, Q. B., Chao, Y., Chen, D., Ye, Z., Liu, Y., and Liou, K. N.: A three-dimensional variational data assimilation system for multiple aerosol species with WRF/Chem and an application to $PM_{2.5}$ prediction, Atmos. Chem. Phys., 13, 4265–4278, doi:10.5194/acp-13-4265-2013, 2013. 27118, 27130, 27131

Mallet, V., Quélo, D., Sportisse, B., Ahmed de Biasi, M., Debry, É., Korsakissok, I., Wu, L., Roustan, Y., Sartelet, K., Tombette, M., and Foudhil, H.: Technical Note: The air quality modeling system Polyphemus, Atmos. Chem. Phys., 7, 5479–5487, doi:10.5194/acp-7-5479-2007, 2007. 27119

Ménard, R., Cohn, S. E., Chang, L.-P., and Lyster, P. M.: Assimilation of stratospheric chemical tracer observations using a Kalman filter. Part I: Formulation, Mon. Weather Rev., 128, 2654–2671, 1999. 27132

Mishchenko, M. I., Travis, L. D., and Lacis, A. A.: Scattering, Absorption, and Emission of Light by Small Particles, Cambridge University Press, 2002. 27123

Nenes, A., Pandis, S., and Pilinis, C.: ISORROPIA: a new thermodynamic equilibrium model for multiphase multi-component inorganic aerosols, Aquat. Geoch., 4, 123–152, 1998. 27124

Nicolet, M.: On the molecular scattering in the terrestrial atmosphere, Planet. Space Sci., 32, 1467–1468, doi:10.1016/0032-0633(84)90089-8, 1984. 27122, 27123

Comparison of lidar observations with aerosol modelling

Y. Wang et al.

Title Page

Abstract	Introduction
Conclusions	References
Tables	Figures

Back | Close

Full Screen / Esc

Printer-friendly Version

Interactive Discussion

Pagowski, M. and Grell, G. A.: Experiments with the assimilation of fine aerosols using an ensemble Kalman filter, J. Geophys. Res., 117, 1–15, doi:10.1029/2012JD018333, 2012. 27118

Pagowski, M., Grell, G. A., Mckeen, S. A., Peckham, S. E., and Devenyi, D.: Three-dimensional variational data assimilation of ozone and fine particulate matter observations: some results using the Weather Research and Forecasting-Chemistry model and Grid-point Statistical Interpolation, Q. J. Roy. Meteor. Soc., 136, 2013–2024, doi:10.1002/qj.700, 2010. 27118, 27131

Péré, J. C., Mallet, M., Pont, V., and Bessagnet, B.: Evaluation of an aerosol optical scheme in the chemistry-transport model CHIMERE, Atmos. Environ., 44, 3688–3699, doi:10.1016/j.atmosenv.2010.06.034, 2010. 27117

Randriamiarisoa, H., Chazette, P., Couvert, P., Sanak, J., and Mégie, G.: Relative humidity impact on aerosol parameters in a Paris suburban area, Atmos. Chem. Phys., 6, 1389–1407, doi:10.5194/acp-6-1389-2006, 2006. 27136

Raut, J., Chazette, P., and Fortain, A.: New approach using lidar measurements to characterize spatiotemporal aerosol mass distribution in an underground railway station in Paris, Atmos. Environ., 43, 575–583, doi:10.1016/j.atmosenv.2008.10.002, 2009a. 27118, 27119

Raut, J., Chazette, P., and Fortain, A.: Link between aerosol optical, microphysical and chemical measurements in an underground railway station in Paris, Atmos. Environ., 43, 860–868, doi:10.1016/j.atmosenv.2008.10.038, 2009b. 27118

Royer, P., Chazette, P., Sartelet, K., Zhang, Q. J., Beekmann, M., and Raut, J.-C.: Comparison of lidar-derived PM_{10} with regional modeling and ground-based observations in the frame of MEGAPOLI experiment, Atmos. Chem. Phys., 11, 10705–10726, doi:10.5194/acp-11-10705-2011, 2011. 27118, 27120, 27127, 27128

Sachdeva, K. and Attri, A. K.: Morphological characterization of carbonaceous aggregates in soot and free fall aerosol samples, Atmos. Environ., 42, 1025–1034, 2007. 27124

Sartelet, K. N., Debry, E., Fahey, K. M., Roustan, Y., Tombette, M., and Sportisse, B.: Simulation of aerosols and gas-phase species over Europe with the Polyphemus system. Part I: model-to-data comparison for 2001, Atmos. Environ., 29, 6116–6131, 2007. 27117, 27119

Sartelet, K. N., Couvidat, F., Seigneur, C., and Roustan, Y.: Impact of biogenic emissions on air quality over Europe and North America, Atmos. Environ., 53, 131–141, doi:10.1016/j.atmosenv.2011.10.046, 2012. 27119

Comparison of lidar observations with aerosol modelling

Y. Wang et al.

Title Page

Abstract	Introduction
Conclusions	References
Tables	Figures

|◄ | ►|

◄ | ►

Back | Close

Full Screen / Esc

Printer-friendly Version

Interactive Discussion

Schaap, M., Spindler, G., Schulz, M., Acker, K., Maenhaut, W., Berner, A., Wieprecht, W., Streit, N., Müller, K., Brüggemann, E., Chi, X., Putaud, J. P., Hitzenberger, R., Puxbaum, H., Baltensperger, U., and ten Brink, H.: Artefacts in the sampling of nitrate studied in the "IN-TERCOMP" campaigns of EUROTRAC-AEROSOL, Atmos. Environ., 48, 6487–6496, 2004. 27117

Seinfeld, J. H. and Pandis, S. N.: Atmospheric Chemistry and Physics, Wiley-Interscience, New York, 1998. 27117

Simpson, D., Fagerli, H., Jonson, J. E., Tsyro, S., Wind, P., and Tuovinen, J. P.: Transboundary acidification, euthrophication and ground level ozone in Europe. Part I: unified EMEP model description, Technical Report, EMEP, 2003. 27117

Skamarock, W. C., Klemp, J. B., Dudhia, J., Gill, D. O., Barker, D. M., Duda, M., Huang, X. Y., Wang, W., and Powers, J. G.: A Description of the Advanced Research WRF Version 3, NCAR Technical Note, available at: http://www.mmm.ucar.edu/wrf/users/docs/arw_v3.pdf (last access: 17 October 2013), 2008. 27120

Stromatas, S., Turquety, S., Menut, L., Chepfer, H., Péré, J. C., Cesana, G., and Bessagnet, B.: Lidar signal simulation for the evaluation of aerosols in chemistry transport models, Geosci. Model Dev., 5, 1543–1564, doi:10.5194/gmd-5-1543-2012, 2012. 27118

Tombette, M., Chazette, P., Sportisse, B., and Roustan, Y.: Simulation of aerosol optical properties over Europe with a 3-D size-resolved aerosol model: comparisons with AERONET data, Atmos. Chem. Phys., 8, 7115–7132, doi:10.5194/acp-8-7115-2008, 2008. 27117, 27120, 27124, 27130

Tombette, M., Mallet, V., and Sportisse, B.: PM_{10} data assimilation over Europe with the optimal interpolation method, Atmos. Chem. Phys., 9, 57–70, doi:10.5194/acp-9-57-2009, 2009. 27118, 27130

Wang, K. C., Dickinson, R. E., and Liang, S. L.: Clear sky visibility has decreased over land globally from 1973 to 2007, Science, 323, 1468–1470, 2009. 27116

Wang, Y., Sartelet, K. N., Bocquet, M., and Chazette, P.: Assimilation of ground versus lidar observations for PM_{10} forecasting, Atmos. Chem. Phys., 13, 269–283, doi:10.5194/acp-13-269-2013, 2013. 27117, 27118, 27127, 27131, 27134

Winker, D. M., Hunt, W. H., Mcgill, M. J., Lidar, C.-A., and Satellite, I. P.: Initial performance assessment of CALIOP, Geophys. Res. Lett., 34, 1–5, doi:10.1029/2007GL030135, 2007. 27117

Title Page

Abstract | Introduction

Conclusions | References

Tables | Figures

|◄ | ►|

◄ | ►

Back | Close

Full Screen / Esc

Printer-friendly Version

Interactive Discussion

Wu, L., Mallet, V., Bocquet, M., and Sportisse, B.: A comparison study of data assimilation algorithms for ozone forecasts, J. Geophys. Res., 113, 1–17, doi:10.1029/2008JD009991, 2008. 27130

Yarwood, G., Rao, S., Yocke, M., and Whitten, G.: Updates to the Carbon Bond Chemical Mechanism: CB05 Final Report to the US EPA, RT-0400675, available at: http://www.camx.com/publ/pdfs/CB05_Final_Report_120805.pdf (last access: 17 October 2013), 2005. 27119

Zhang, Y., Sartelet, K., Zhu, S., Wang, W., Wu, S.-Y., Zhang, X., Wang, K., Tran, P., Seigneur, C., and Wang, Z.-F.: Application of WRF/Chem-MADRID and WRF/Polyphemus in Europe – Part 2: Evaluation of chemical concentrations and sensitivity simulations, Atmos. Chem. Phys., 13, 6845–6875, doi:10.5194/acp-13-6845-2013, 2013. 27120

Comparison of lidar observations with aerosol modelling

Y. Wang et al.

Title Page

Abstract | Introduction

Conclusions | References

Tables | Figures

|◀ | ▶|

◀ | ▶

Back | Close

Full Screen / Esc

Printer-friendly Version

Interactive Discussion

Table 1. Dry CRI and density for different aerosol species at $\lambda = 355$ nm. Re (resp. Im) stands for the real (resp. imaginary) part of CRI.

Species	Re	Im	density (g cm^{-3})
Nitrate	1.53	−0.005	1.5
Ammonium	1.53	−0.005	0.91
Black carbon	1.75	−0.4645	2.25
Mineral dust	1.53	−0.0166	2.33
Organics	1.53	−0.008	1.3
Sulfate	1.45	-1×10^{-8}	1.84
Sodium	1.509	-2.946×10^{-7}	0.97
Chlorate	1.509	-2.946×10^{-7}	1.15
Water	1.35738	2.72875×10^{-8}	1.0

Title Page

Abstract | Introduction

Conclusions | References

Tables | Figures

◄ | ►

◄ | ►

Back | Close

Full Screen / Esc

Printer-friendly Version

Interactive Discussion

Table 2. Statistics (see Appendix A) of the simulation results for the Airparif network during the MEGAPOLI summer experiment. Obs. stands for observation. Sim. stands for simulation. Corr. stands for correlation.

Day	PM_{10}						$PM_{2.5}$					
	Obs. mean	Sim. mean	RMSE	Corr.	MFB	MFE	Obs. mean	Sim. mean	RMSE	Corr.	MFB	MFE
	$\mu g\,m^{-3}$	$\mu g\,m^{-3}$	$\mu g\,m^{-3}$	%	%	%	$\mu g\,m^{-3}$	$\mu g\,m^{-3}$	$\mu g\,m^{-3}$	%	%	%
All	21.53	14.14	10.79	64	−42	49	12.59	12.78	6.02	68	4	39
1	44.99	29.39	18.08	78	−45	47	28.82	27.14	7.94	74	−10	23
4	18.37	11.11	8.34	8	−48	48	10.80	9.99	3.90	−25	−4	31
16	26.25	16.47	12.28	16	−41	46	12.60	15.76	5.41	31	25	34
21	27.84	16.84	13.13	28	−46	50	15.46	16.19	5.84	14	6	31
26	18.04	10.12	9.52	−4.6	−52	53	12.32	10.27	5.05	7.1	−16	34
29	29.25	12.33	18.49	28	−76	78	14.82	11.78	7.32	38	−20	37

Table 3. Statistics (see Appendix A) of the simulation results for the AERONET network for different lidar measurement days.

Day	Obs. mean	Sim. mean	RMSE	Corr. %	MFB %	MFE %
1	0.59	0.47	0.20	−8	−21	29
4	0.25	0.14	0.12	37	−58	58
16	0.26	0.18	0.08	80	−33	33
26	0.15	0.08	0.07	45	−53	53

Full Screen / Esc

Printer-friendly Version

Interactive Discussion

Table 4. Statistics (see Appendix A) of the simulation results (PM_{10} and $PM_{2.5}$) without DA and with DA for the Airparif network for 1 and 26 July 2009. "With DA (PM_{10})" stands for the assimilation of lidar observations correcting directly PM_{10}. "With DA ($PM_{2.5}$ and $PM_{2.5-10}$)" stands for the assimilation of lidar observations correcting separately $PM_{2.5}$ and $PM_{2.5-10}$.

Day	Species	Sim.	Obs. mean	Sim. mean	RMSE	Corr. %	MFB %	MFE %
1	PM_{10}	Without DA	47.26	32.35	17.74	84	−41	43
		With DA (PM_{10})		36.20	13.69	90	−29	32
		With DA ($PM_{2.5}$ and $PM_{2.5-10}$)		39.85	11.63	84	−19	25
	$PM_{2.5}$	Without DA	30.52	30.21	8.54	69	−5	23
		With DA (PM_{10})		33.04	10.44	59	5	27
		With DA ($PM_{2.5}$ and $PM_{2.5-10}$)		33.08	10.45	58	5	27
26	PM_{10}	Without DA	16.25	9.96	6.67	−20	−47	47
		With DA (PM_{10})		10.55	6.08	15	−42	42
		With DA ($PM_{2.5}$ and $PM_{2.5-10}$)		12.80	4.73	26	−25	30
	$PM_{2.5}$	Without DA	10.25	8.99	2.80	7	−9	25
		With DA (PM_{10})		9.64	2.51	22	−2	22
		With DA ($PM_{2.5}$ and $PM_{2.5-10}$)		9.49	2.54	21	−4	22
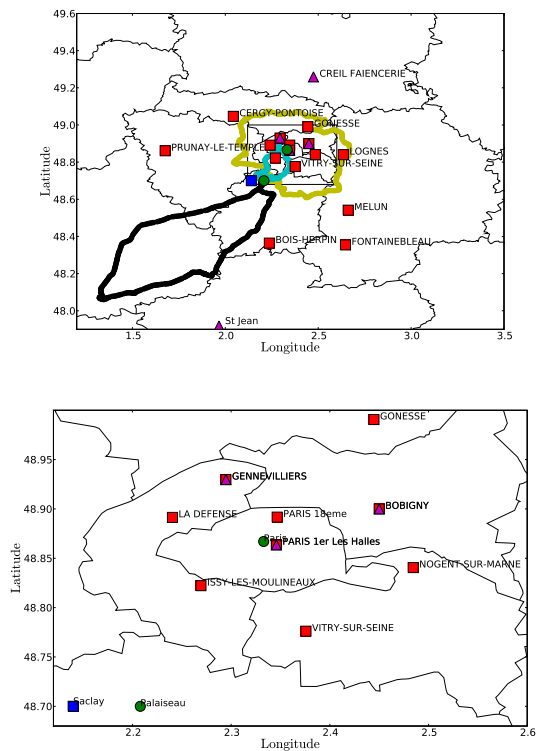
Fig. 1. The blue square shows the location of the ground-based in situ lidar station, the red squares (resp. the magenta triangles) show the locations of Airparif stations for PM_{10} (resp. $PM_{2.5}$) measurements and the green discs show the locations of AERONET stations. The black pattern shows the GBML track on 1 July 2009. The yellow and cyan patterns show two GBML tracks on 26 July 2009. The rectangle area is detailed in the bottom figure.

Comparison of lidar observations with aerosol modelling

Y. Wang et al.

Printer-friendly Version

Interactive Discussion
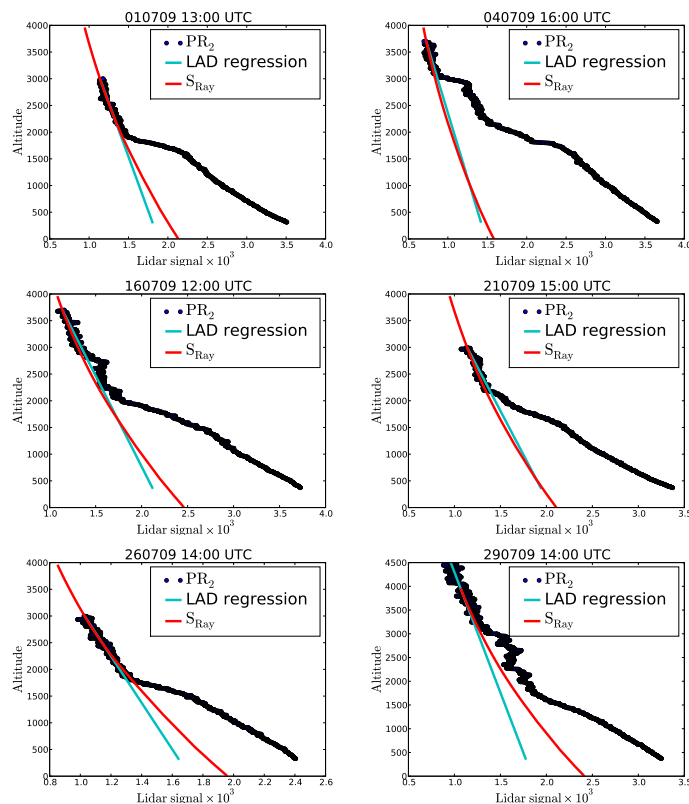
Fig. 2. Blue points (resp. red lines) indicate lidar signals PR$_2$ (resp. simulated molecular signals S_{Ray}) at 13:00 UTC 1, 16:00 UTC 4, 12:00 UTC 16, 15:00 UTC 21, 14:00 UTC 26 and 14:00 UTC 29 July 2009 (blue points). LAD regressions of weighted lidar measurement points are indicated by cyan lines.
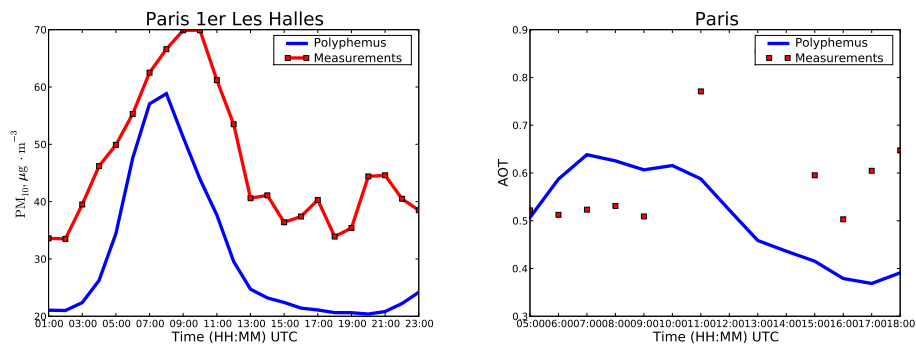
Fig. 3. Left (resp. right) figure shows the hourly evolution of the PM_{10} concentration (resp. AOD) at station Paris for 1 July 2009.

Printer-friendly Version

Interactive Discussion
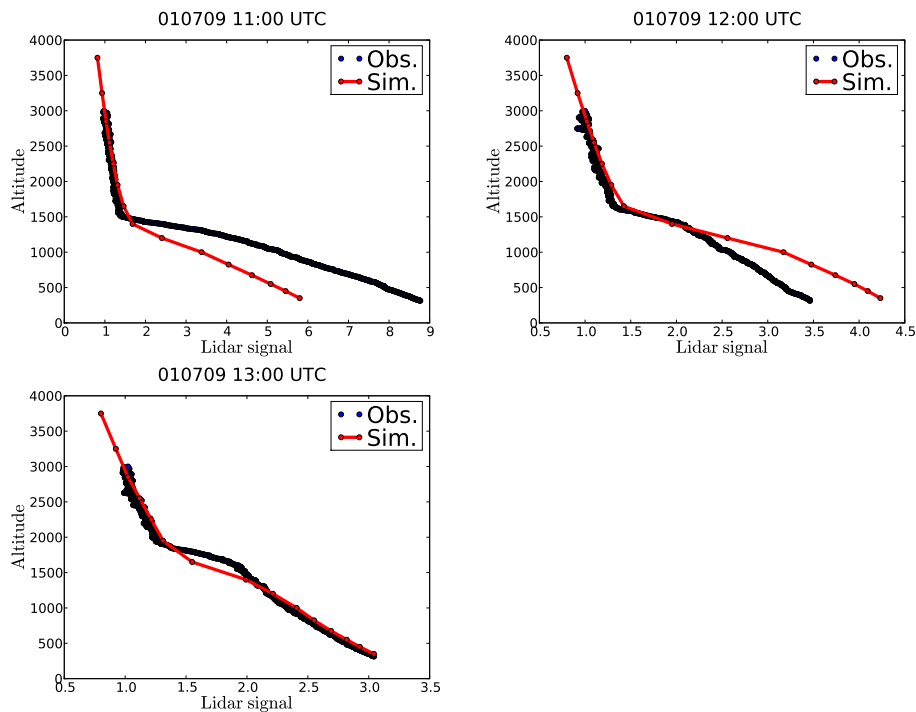
Fig. 4. Comparisons between the vertical profiles observed by GBML (blue points) and simulated by POLYPHEMUS (red lines) on 1 July 2009 from 11:00 to 13:00 UTC. Lidar observations below the altitude of full overlap are not represented.
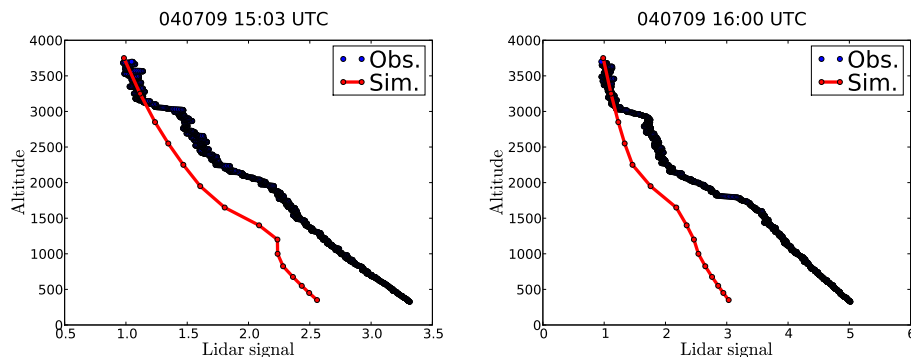
Fig. 5. Comparisons between the vertical profiles observed by GBML (blue points) and simulated by POLYPHEMUS (red lines) on 4 July 2009 at 15:03 and 16:00 UTC. Lidar observations below the altitude of full overlap are not represented.
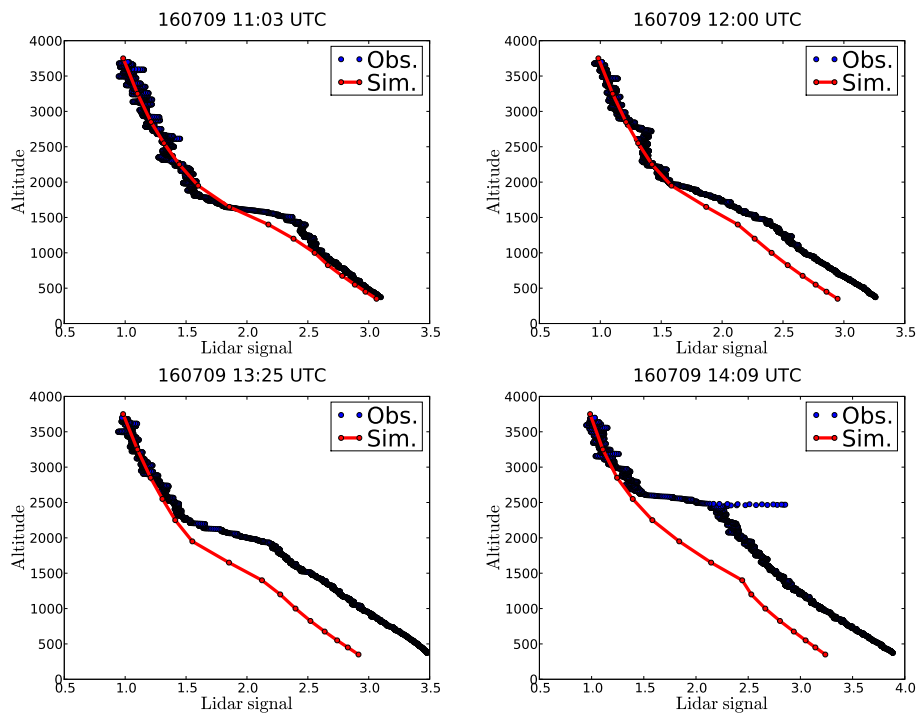
Fig. 6. Comparisons between the vertical profiles observed by GBML (blue points) and simulated by POLYPHEMUS (red lines) on 16 July 2009 at 11:03, 12:00, 13:25 and 14:09 UTC. Lidar observations below the altitude of full overlap are not represented.
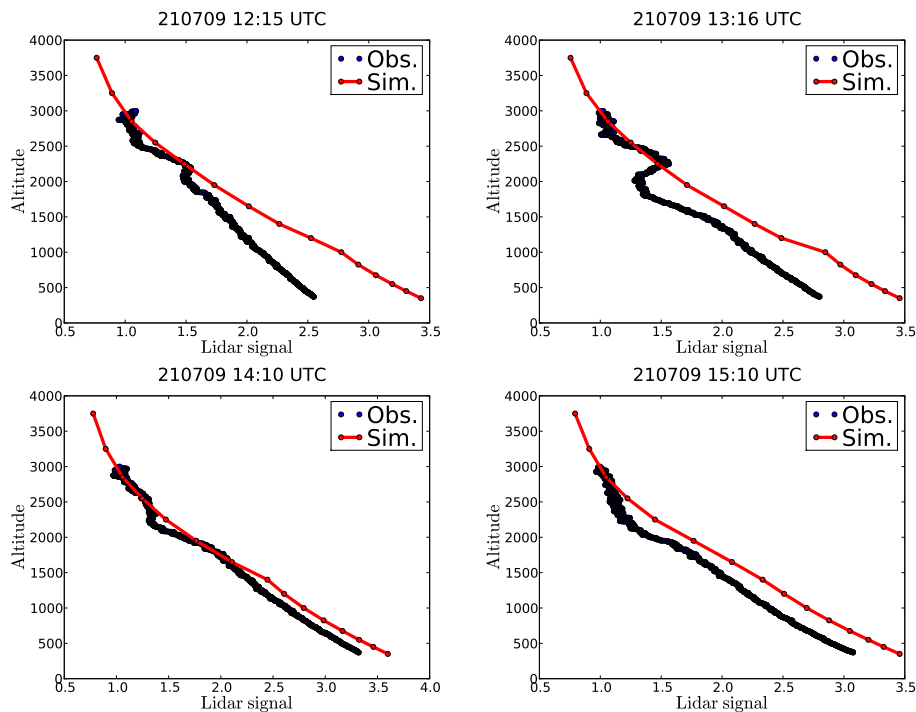
Fig. 7. Comparisons between the vertical profiles observed by GBML (blue points) and simulated by Polyphemus (red lines) on 21 July 2009 at 12:15, 13:16, 14:10 and 15:10 UTC. Lidar observations below the altitude of full overlap are not represented.
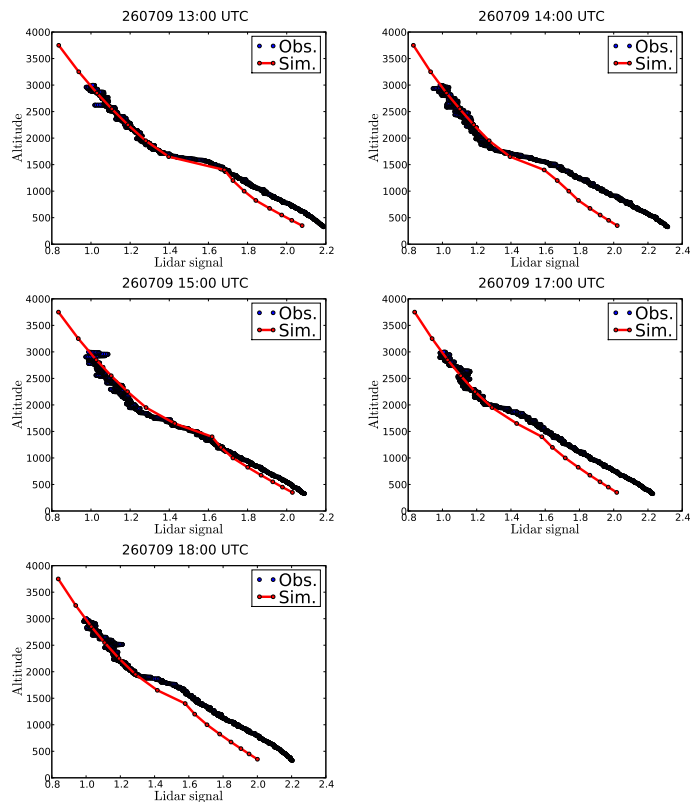
Fig. 8. Comparisons between the vertical profiles observed by GBML (blue points) and simulated by POLYPHEMUS (red lines) on 26 July 2009 at 13:00, 14:00, 15:00, 17:00 and 18:10 UTC. Lidar observations below the altitude of full overlap are not represented.
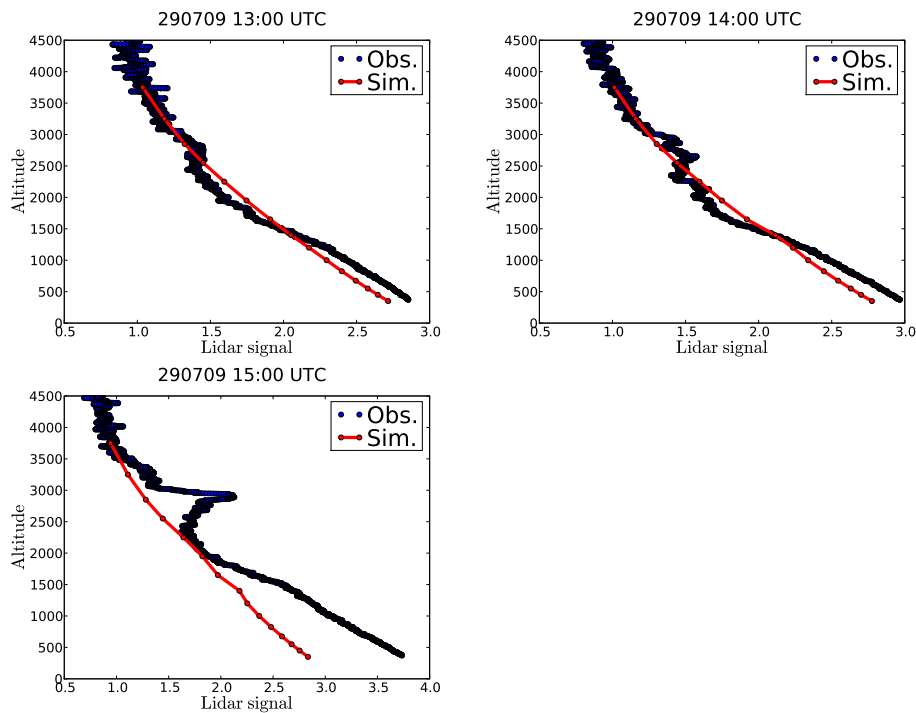
Fig. 9. Comparisons between the vertical profiles observed by GBML (blue points) and simulated by POLYPHEMUS (red lines) on 26 July 2009 at 13:00, 14:00 and 15:00 UTC. Lidar observations below the altitude of full overlap are not represented.
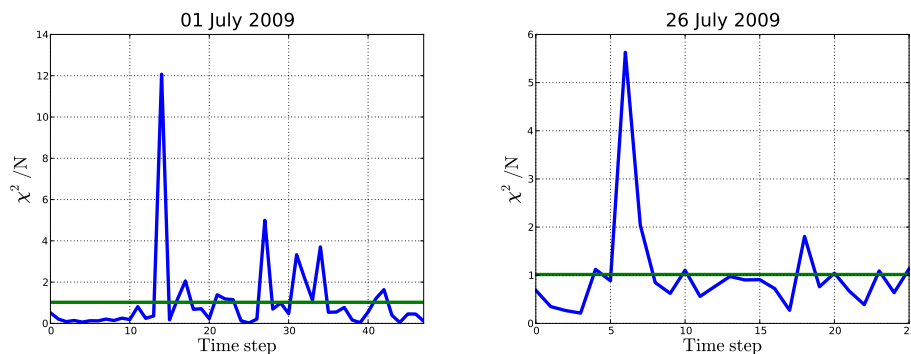
Fig. 10. Time evolutions of χ^2/N (blue lines) for DA runs on 1 and 26 July 2009. The mean over DA window of χ^2/N is 1.02 (resp. 1.02) for 1 (resp. 26) July 2009.
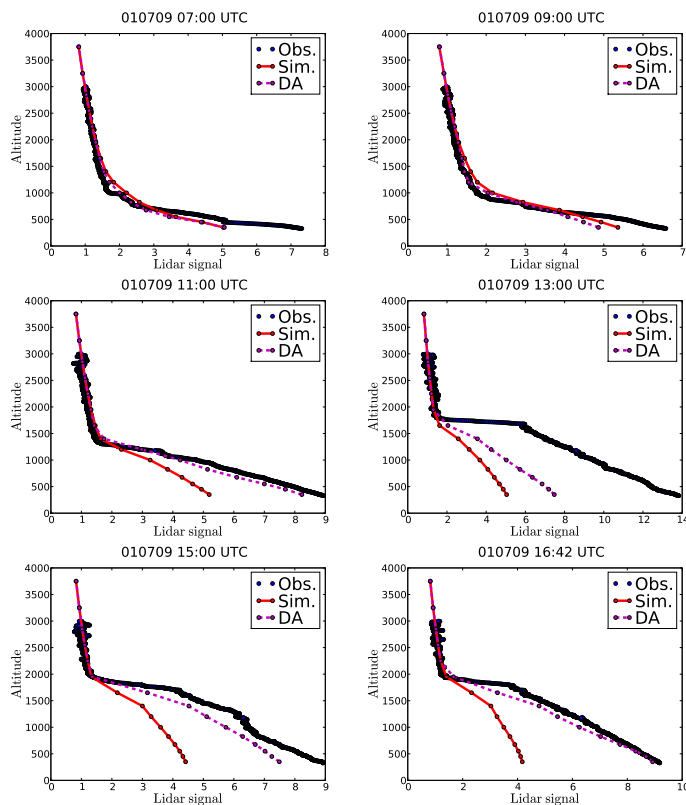
Fig. 11. Lidar vertical profiles observed by the ground-based in situ lidar at Saclay (blue points), simulated without DA (red lines) and simulated with DA (magenta lines) on 1 July 2009.